

# Supplementary Material for “Color Control Functions for Multiprimary Displays II: Variational Robustness Optimization”

Carlos Eduardo Rodríguez-Pardo and Gaurav Sharma, *Fellow, IEEE*

This document provides supplementary material, for the paper [1]. In Section S.I, we discuss the convergence of the Algorithm 1. In Section S.II, we provide details about computation of the random CCF. In Section S.III, we specify the tristimulus values for the primaries and the primary variations of the displays designs used for evaluation of CCFs, as well as the CBS bases used for the visualizations. In Section S.IV, we augment the quantitative metrics reported in Tables I– III for characterizing the performance for alternative CCFs for the different multiprimary designs by tabulating the  $\Delta E$  color differences computed using other color difference formulae. In Section S.V, we provide additional visual assessments of the proposed CCFs along different color trajectories. Section S.VI presents results for two additional systems of primaries that illustrate the general applicability of the proposed methodology.

## S.I. CONVERGENCE OF THE PROPOSED ALGORITHM FOR COMPUTING ROBUST CCFs

The convergence of Algorithm 1 to  $\alpha_{\Gamma}^{\mathcal{F}}(\cdot)$ , the unique optimal solution of (1), is independent of the initialization conditions, but the number of iterations required to reach this point may differ. Figure S.1, shows the CBS representation of  $\alpha_n^{\mathcal{F}}(\cdot)$ , for different iterations ( $n$ ) of Algorithm 1, along the radial line in CIELUV at constant lightness,  $\tau_L = 75$ , and opposing CIELUV hues corresponding to  $h_{\mathcal{T}} = 86^\circ$  and  $h_{\mathcal{T}} = 266^\circ$  for the four primary system  $\mathbf{P}_R^{(4)}$ . The plots are shown as functions of chroma  $C_{\mathcal{T}}$ , to distinguish between the two hues, we add a negative sign to the chroma values for the points with  $h_{\mathcal{T}} = 266^\circ$ , leaving a positive sign for the points with  $h_{\mathcal{T}} = 86^\circ$ . We considered two different initializations  $\alpha_0^{\mathcal{F}}(\cdot)$ : the axially linear CCF (Fig. S.1(a)), and the random CCF (Fig. S.1(b)). Fig. S.1 shows that despite the prominent differences between the initializations, the sequence  $\alpha_n^{\mathcal{F}}(\cdot)$  tends the same point, but the number of iterations required differs significantly. Initialization with the axially linear CCF, i.e.,  $\alpha_0^{\mathcal{F}}(\cdot) = \alpha_{\mathcal{A}}^{\mathcal{F}}(\cdot)$ , quickly leads to convergence, whereas initialization with the random

C.E. Rodríguez-Pardo is with the Department of Electrical and Computer Engineering, University of Rochester, Rochester, NY, 14627 USA (e-mail: c.rodriguezpardo@rochester.edu)

G. Sharma is with the Department of Electrical and Computer Engineering, Department of Computer Science, and Department of Biostatistics and Computational Biology, University of Rochester, Rochester, NY 14627, USA (e-mail: gaurav.sharma@rochester.edu)

CCF, i.e.,  $\alpha_0^{\mathcal{F}}(\cdot) = \alpha_{\sim}^{\mathcal{F}}(\cdot)$ , requires more iterations for convergence due to the random variations in the random CCF  $\alpha_{\sim}^{\mathcal{F}}(\cdot)$  everywhere in the gamut.

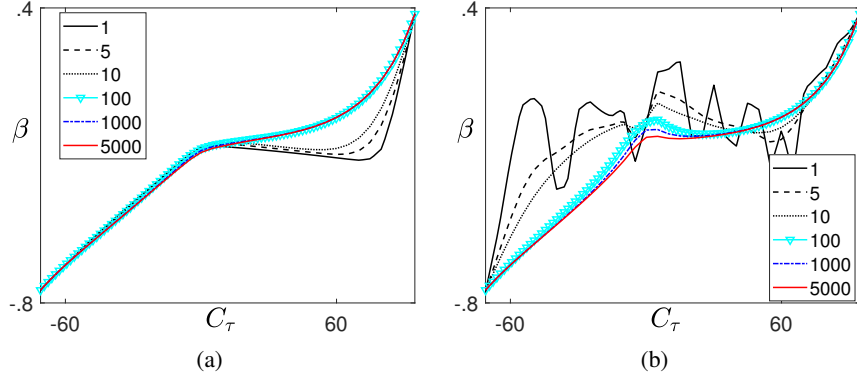


Fig. S.1: Convergence of projected gradient descent algorithm for different initializations. Algorithm 1 was run twice with same parameters but different initializations. For (a) the initialization used  $\alpha_0^{\mathcal{F}}(\cdot) = \alpha_{\mathcal{A}}^{\mathcal{F}}(\cdot)$ , the axially linear CCF, while for (b) the initialization used  $\alpha_0^{\mathcal{F}}(\cdot) = \alpha_{\sim}^{\mathcal{F}}(\cdot)$ , the random CCF. The plots show CBS visualizations for  $\alpha_n^{\mathcal{F}}$  at different values of iteration number  $n$ , along a radial line in CIELUV at constant lightness,  $\tau_L = 75$ , and opposing CIELUV hues corresponding to  $h_{\tau} = 86^{\circ}$  and  $h_{\tau} = 266^{\circ}$ , for the four primary system  $\mathbf{P}_R^{(4)}$ . The CBS representations are presented as function of chroma  $C_{\tau}$ , rendering of the ramp between the maximum chroma values for the two opposing hues  $h_{\tau} = 86^{\circ}/266^{\circ}$ . For the purpose of illustration, chroma values along the two opposing hues  $h_{\tau} = 86^{\circ}/266^{\circ}$  are assigned positive and negative signs, respectively.

## S.II. GENERATING THE RANDOM CCF

To construct the random CCF  $\alpha_{\sim}^{\mathcal{F}}(\cdot)$ , we take advantage of the fact that the MCS lies within a  $(K-3)$ -dimensional affine subspace. We consider an “orthogonal” polytope containing the CBS representation for the vertices of the MCS, which for the case of  $K = 4, 5$ , and  $6$ , corresponds to a line, a rectangle, and a cuboid. To obtain samples that are distributed uniformly over the irregularly shaped MCS polytope, we generate samples uniformly distributed in the orthogonal enclosing polytope, and retain only those that fall inside the MCS. Figure S.2 illustrates the process for two tristimuli in the gamut of the five primary system  $\mathbf{P}_U^{(5)}$ . For the results presented in the main paper and in this Supplementary Materials document, the random CCF  $\alpha_{\sim}^{\mathcal{F}}(\cdot)$  was evaluated using the methodology described in this section. Also, the random CCF  $\alpha_{\sim}^{\mathcal{F}}(\cdot)$  was directly evaluated (without using a LUT) for all the numerical metrics reported and visualizations presented, except for the global and local lack of smoothness metrics  $\Theta^*$  and  $\mathcal{M}_{\Theta}^*(\tau)$ , which, for consistency, used a LUT representation of the random CCF with the same sampling grid as the other CCFs. In the latter setting, the methodology described here was still used for obtaining the values for the random CCF  $\alpha_{\sim}^{\mathcal{F}}(\cdot)$  at the LUT nodes.

## S.III. SPECIFICATIONS OF PRIMARY DESIGNS FOR BENCHMARKING AND PRIMARY VARIATIONS

Table S.I lists the tristimulus values for the primaries of the multiprimary display systems introduced in Section V-A and used for the evaluation of CCFs. Table S.II lists the variations in the primaries used for the assessments

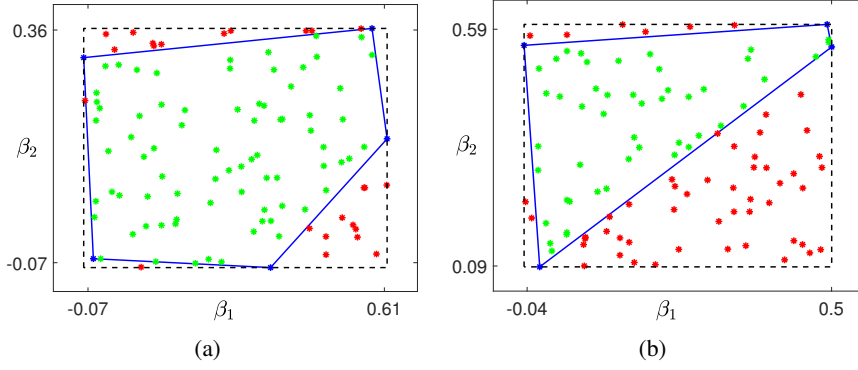


Fig. S.2: Computation of the CCF  $\alpha_{\sim}^{\mathcal{F}}(\boldsymbol{\tau})$  for CIELUV colors (a)  $\boldsymbol{\tau} = [40, 0, 0]^T$  and (b)  $\boldsymbol{\tau} = [40, 70, 0]^T$  in the gamut of the five primary display  $\mathbf{P}_U^{(5)}$ . For each of the subfigures (a) and (b), the blue polygon is the CBS representation for the MCS  $\Omega(\mathbf{t})$ , a convex set whose vertices are also plotted in blue. In this setting, the orthogonal polytope enclosing the MCS is the rectangle shown by the dashed black line. To generate a point uniformly distributed over the MCS, we generate a point that is uniformly distributed over the rectangle shown by the dashed black line, if the generated point is inside the MCS, it is retained as the value for  $\alpha_{\sim}^{\mathcal{F}}(\boldsymbol{\tau})$ , otherwise, the point is discarded and the process is repeated (till the generated point lies inside the MCS). For illustration, subfigures (a) and (b) also include a number of points generated uniformly over their corresponding enclosing rectangles, where the points inside the MCS are plotted in green, and those outside are plotted in red.

of CCF robustness in the visual examples presented in various figures. Within Table S.II, we also identify the figures from the main paper or the Supplementary Material where visual examples were presented using the corresponding primary variations.

We rely on the selection of an orthonormal basis of the CBS for the visualization of the CCFs. We obtain this basis by computing the SVD decomposition  $\mathbf{P} = \mathbf{U}\mathbf{S}\mathbf{V}^T$  of the primary matrix  $\mathbf{P}$ , where  $\mathbf{S}$  is a  $3 \times K$  diagonal matrix containing the singular values of  $\mathbf{P}$ , and  $\mathbf{U}$ ,  $\mathbf{V}$  are  $3 \times 3$  and  $K \times K$  orthonormal matrices whose columns are orthonormal basis for  $\mathbb{R}^3$  and  $\mathbb{R}^K$ , respectively. In particular, the last  $(K - 3)$  columns of the matrix  $\mathbf{V} = [\mathbf{v}_1, \dots, \mathbf{v}_K]$  form an orthonormal basis for the null space (CBS) of  $\mathbf{P}$  [2]. Therefore, we set the basis matrix  $\mathbf{B} \stackrel{\text{def}}{=} [\mathbf{b}_1, \dots, \mathbf{b}_{K-3}]$ , so  $\mathbf{b}_1 = \mathbf{v}_4, \dots, \mathbf{b}_{K-3} = \mathbf{v}_K$ . The bases for the primary systems we obtain for each primary system using this procedure are shown in Table S.III.

#### S.IV. QUANTITATIVE $\Delta E$ METRICS FOR ALTERNATIVE CCFs USING OTHER COLOR DIFFERENCE FORMULAE

For characterizing the performance for alternative CCFs for the different multiprimary designs, one of the metrics reported in Tables I– III was the Euclidean distance, the  $\Delta E$  computed in CIELUV space, which is technically referred to as  $\Delta E_{uv}^*$  [3]. Alternative computations of color differences are also commonly used in the literature, several of which have been developed more recently with the objective of providing better perceptual uniformity. We therefore augment the quantitative metrics reported in Tables I– III by tabulating corresponding  $\Delta E$  color differences computed using other color difference formulae. Specifically, in Tables S.IV– S.VI, using an organization identical to Tables I– III, respectively, we report three additional color differences, specifically: (a)  $\Delta E_{ab}^*$ , the Euclidean color

		<b>P1</b>	<b>P2</b>	<b>P3</b>	<b>P4</b>	<b>P5</b>	<b>P6</b>
$\mathbf{P}_R^{(4)}$	X	0.5197	0.1661	0.0323	0.1447		
	Y	0.2502	0.3995	0.2118	0.0465		
	Z	0.0000	0.0193	0.1268	0.8422		
$\mathbf{P}_U^{(4)}$	X	5.1798	35.2189	30.3396	78.0246		
	Y	82.0848	13.0499	2.8297	58.5511		
	Z	12.5958	0.0001	156.4330	1.3366		
$\mathbf{P}_M^{(4)}$	X	108075	241193	23023	85004		
	Y	45219	288628	147404	12483		
	Z	14	3392	114378	450264		
$\mathbf{P}_U^{(5)}$	X	74.4791	26.2566	4.7420	2.4408	40.1894	
	Y	65.8501	1.3224	60.3915	13.2309	15.0332	
	Z	0.1831	129.2980	9.8782	30.2490	0.0003	
$\mathbf{P}_M^{(5)}$	X	109703	139604	30359	28270	67988	
	Y	51750	140629	138511	34677	5604	
	Z	39	2005	20020	191684	345370	
$\mathbf{P}_U^{(6)}$	X	97.1196	20.4393	4.5604	2.1937	35.6898	7.8037
	Y	85.8675	1.0294	58.0786	11.8917	13.3501	6.3341
	Z	0.2387	100.6512	9.4999	27.1872	0.0003	54.5976

TABLE S.I: Tristimulus values of the primaries of the display systems used for the evaluation of the CCFs. Note that the primary tristimuli are not uniformly normalized and retain the scaling from the sources from which these are adopted.

		$\Delta\mathbf{p}_1$	$\Delta\mathbf{p}_2$	$\Delta\mathbf{p}_3$	$\Delta\mathbf{p}_4$	$\Delta\mathbf{p}_5$	$\Delta\mathbf{p}_6$
$\Delta\mathbf{P}_R^{(4)}$ Fig 6(a)	X	-0.0561	0.0259	-0.0193	0.0438		
	Y	-0.0106	-0.0342	0.0154	-0.0725		
	Z	-0.0060	-0.0037	0.0000	0.0031		
$\Delta\mathbf{P}_R^{(4)}$ Fig S.3(a)	X	0.0151	-0.0056	0.0117	-0.0011		
	Y	-0.0237	0.0124	-0.0041	0.0427		
	Z	-0.0063	-0.0168	-0.0003	-0.0032		
$\Delta\mathbf{P}_R^{(4)}$ Fig S.5	X	0.0303	-0.0112	0.0235	-0.0021		
	Y	-0.0474	0.0249	-0.0083	0.0853		
	Z	-0.0126	-0.0337	-0.0006	-0.0064		
$\Delta\mathbf{P}_U^{(5)}$ Fig 5	X	3.1528	4.4725	-0.4831	-1.1236	-1.4986	
	Y	-3.7510	-4.7413	-2.7206	1.1291	1.4422	
	Z	-0.2632	0.4772	-1.1850	-0.0430	-0.1245	
$\Delta\mathbf{P}_M^{(5)}$ Fig 6(b)	X	-7777	16548	-8908	2969	1970	
	Y	9048	-10697	10095	250	1024	
	Z	2140	2102	4880	3258	3420	
$\Delta\mathbf{P}_U^{(6)}$ Fig S.3(b)	X	4.3799	2.2485	-0.6922	-1.0358	-1.3543	-2.6376
	Y	1.7856	-2.6122	0.5066	0.9972	1.2835	0.6606
	Z	-1.9937	3.6905	0.0891	0.1611	0.0126	0.3082
$\Delta\mathbf{P}_U^{(6)}$ Fig S.4	X	9.0435	4.2502	-5.0570	-1.7291	-2.7226	3.8999
	Y	-9.1573	-7.9337	2.9464	1.1716	2.5630	0.6093
	Z	-1.1009	4.8507	0.2041	1.6015	0.4324	-0.8318

TABLE S.II: Variations in the primaries used for the assessments of CCF robustness in the visual examples presented in Section VI of the paper [1] and in Section S.V. The table also identifies the figures where visual examples were presented using the corresponding primary variations.

	$\mathbf{b}_1$	$\mathbf{b}_2$	$\mathbf{b}_3$
$\mathbf{B}_R^{(4)}$	-0.1462		
	0.5202		
	-0.8337		
	0.1136		
$\mathbf{B}_U^{(4)}$	-0.1515		
	-0.8984		
	0.0087		
	0.4122		
$\mathbf{B}_M^{(4)}$	-0.7962		
	0.3605		
	-0.4716		
	0.1171		
$\mathbf{B}_U^{(5)}$	0.0378	-0.4606	
	-0.2018	-0.0340	
	-0.2524	0.2818	
	0.9450	0.0561	
	0.0342	0.8391	
$\mathbf{B}_M^{(5)}$	-0.1365	-0.6927	
	0.2301	0.5730	
	-0.3631	-0.2534	
	0.7886	-0.3073	
	-0.4180	0.1820	
$\mathbf{B}_U^{(6)}$	0.0298	-0.3335	0.0425
	-0.1839	-0.0683	-0.4542
	-0.2287	0.2714	-0.1371
	0.9507	0.0531	-0.0343
	0.0157	0.8971	-0.0279
	-0.0946	0.0538	0.8781

TABLE S.III: Orthonormal bases for the CBS of the multiprimary displays used in the visualization of the CCFs in Section VI of the main paper [1] and in Section S.V.

difference in CIELAB [3], (b)  $\Delta E_{00}^*$ , the CIEDE2000 color difference [4]–[6], and (c)  $\Delta E_{16}$ , the color difference in CAM16-UCS [7] computed with recommended parameter settings for a dark surround and with the luminance of the test adapting field set to 12.73 candela per square meter as 20% of the display white luminance for a 200 lux display. Note that the  $\Delta E_{16}$  values for the axially linear CCF  $\alpha_{\mathcal{A}}^{\mathcal{F}}(\cdot)$  are not exactly zero but are zero upto the reported significant digits. Note that the  $L^*$  axis is the same for CIELAB and CIELUV, so the values for the  $\Delta E_{uv}^*$  and  $\Delta E_{ab}^*$  color differences also exhibit good absolute consistency for these metrics, because our reported errors are in the vicinity of the gray axes. These additional numerical results reinforce the overall trends and conclusions based on the results presented in the main paper.

#### S.V. ADDITIONAL TRAJECTORIES FOR VISUAL ASSESSMENTS

In this section, we present renderings of additional color trajectories that complement the results presented in the main paper [1].

CCF	$\mathbf{P}_R^{(4)}$						$\mathbf{P}_U^{(4)}$						$\mathbf{P}_M^{(4)}$					
	$\Delta E_{ab}^*$		$\Delta E_{00}^*$		$\Delta E_{16}$		$\Delta E_{ab}^*$		$\Delta E_{00}^*$		$\Delta E_{16}$		$\Delta E_{ab}^*$		$\Delta E_{00}^*$		$\Delta E_{16}$	
	av.	max	av.	max	av.	max	av.	max	av.	max	av.	max	av.	max	av.	max	av.	max
$\alpha_{\sim}^{\mathcal{F}}$	0.63	6.30	0.85	7.73	0.98	4.37	0.64	6.99	0.86	8.44	0.97	4.76	0.83	10.56	1.10	11.62	1.09	5.58
$\alpha_{\Gamma}^{\mathcal{F}}$	0.00	0.02	0.00	0.02	0.01	0.26	0.00	0.02	0.00	0.02	0.01	0.26	0.01	0.06	0.01	0.08	0.07	0.52
$\alpha_{\Theta}^{\mathcal{F}}$	0.00	0.07	0.01	0.11	0.05	0.52	0.02	0.11	0.02	0.16	0.11	0.63	0.02	0.21	0.03	0.31	0.13	1.22
$\alpha_A^{\mathcal{F}}$	0.00	0.00	0.00	0.00	0.00	0.00	0.00	0.00	0.00	0.00	0.00	0.00	0.00	0.00	0.00	0.00	0.00	0.00
$\alpha_{\mu}^{\mathcal{F}}$	0.31	1.97	0.42	2.73	0.66	2.22	0.48	2.84	0.66	3.86	0.88	2.99	0.63	4.34	0.85	5.63	0.99	3.47
$\alpha_{p-}^{\mathcal{F}}$	1.27	7.61	1.67	8.99	1.60	4.82	1.17	6.30	1.55	7.72	1.52	4.40	1.50	9.36	1.96	10.59	1.70	5.41
$\alpha_{p+}^{\mathcal{F}}$	1.69	10.46	2.18	11.50	1.89	5.44	1.85	10.53	2.38	11.59	1.99	5.69	2.41	15.91	3.00	15.42	2.26	6.66

TABLE S.IV: Quantitative metrics for gray axis invariance for alternative CCFs for the  $K = 4$  primary display systems  $\mathbf{P}_R^{(4)}$ ,  $\mathbf{P}_U^{(4)}$  and  $\mathbf{P}_M^{(4)}$ . The CCFs obtained with the proposed variational approaches are identified (in this and subsequent tables) by yellow highlighting of the corresponding rows.

CCF	$\mathbf{P}_U^{(5)}$						$\mathbf{P}_M^{(5)}$					
	$\Delta E_{ab}^*$		$\Delta E_{00}^*$		$\Delta E_{16}$		$\Delta E_{ab}^*$		$\Delta E_{00}^*$		$\Delta E_{16}$	
	av.	max	av.	max	av.	max	av.	max	av.	max	av.	max
$\alpha_{\sim}^{\mathcal{F}}$	1.95	17.12	2.47	15.90	2.02	7.29	2.22	18.26	2.79	16.78	2.19	7.34
$\alpha_{\Gamma}^{\mathcal{F}}$	0.09	0.32	0.08	0.37	0.29	0.91	0.08	0.32	0.07	0.39	0.27	0.96
$\alpha_{\Theta}^{\mathcal{F}}$	0.63	3.81	0.85	4.93	1.07	3.65	0.50	3.85	0.67	5.04	0.91	3.84
$\alpha_A^{\mathcal{F}}$	0.00	0.00	0.00	0.00	0.00	0.00	0.00	0.00	0.00	0.00	0.00	0.00
$\alpha_{\mu}^{\mathcal{F}}$	0.91	6.08	1.22	7.36	1.32	4.41	0.71	4.47	0.96	5.76	1.12	3.47
$\alpha_{p-}^{\mathcal{F}}$	1.59	9.37	2.06	10.49	1.83	5.16	3.00	18.99	3.68	17.18	2.63	7.65
$\alpha_{p+}^{\mathcal{F}}$	3.02	18.98	3.65	16.94	2.61	7.63	3.38	21.64	4.07	18.48	2.83	8.11

TABLE S.V: Quantitative metrics for gray axis invariance for alternative CCFs for the  $K = 5$  primary display systems  $\mathbf{P}_U^{(5)}$  and  $\mathbf{P}_M^{(5)}$ .

Figure S.3 shows renderings of the gray axis for the display systems  $\mathbf{P}_R^{(4)}$  and  $\mathbf{P}_U^{(6)}$ . Below the legend labels identifying the alternative CCFs considered, the first  $(K - 3)$  plots at the top of Fig. 5 show for each CCF the corresponding CBS components as function of the lightness  $\tau_L$ . Below these plots, there are a series of stripes representing display renderings of the gray axis. The first one represents the rendering obtained by any CCF driving the display in the absence of primary variations, i.e., with the nominal primaries, while the remaining stripes show

CCF	$\mathbf{P}_U^{(6)}$					
	$\Delta E_{ab}^*$		$\Delta E_{00}^*$		$\Delta E_{16}$	
	av.	max	av.	max	av.	max
$\alpha_{\sim}^{\mathcal{F}}$	1.73	12.43	2.23	13.00	1.93	6.09
$\alpha_{\Gamma}^{\mathcal{F}}$	0.09	0.34	0.08	0.37	0.29	0.79
$\alpha_{\Theta}^{\mathcal{F}}$	0.89	5.33	1.19	6.56	1.31	4.26
$\alpha_A^{\mathcal{F}}$	0.00	0.00	0.00	0.00	0.00	0.00
$\alpha_{\mu}^{\mathcal{F}}$	0.86	4.85	1.16	6.07	1.28	3.90
$\alpha_{p-}^{\mathcal{F}}$	2.49	15.06	3.12	14.82	2.40	6.80
$\alpha_{p+}^{\mathcal{F}}$	3.00	17.70	3.67	16.45	2.64	7.21

TABLE S.VI: Quantitative metrics for gray axis invariance for alternative CCFs for the  $K = 6$  primary display system  $\mathbf{P}_U^{(6)}$ .

the results obtained when each of the evaluated CCFs is used to drive the display in the presence of primary variations. In this case, each primary underwent a variation equivalent to 5% of the primary's norm<sup>1</sup>. The graph below the stripes shows, as a function of the lightness  $\tau_L$ , the perceptual difference  $\Delta E(\cdot)$  between the gray axis renderings with and without primary variations (from their nominal values). Finally, below this graph there are two plots in the  $\tau_L - \tau_{c_1}$  and  $\tau_L - \tau_{c_2}$  planes depicting the desired values on the gray axis (shown by the black line) and the renderings obtained with the alternative CCFs in the presence of the primary variations.

Note from Fig. S.3(a), that the plots of CBS components of  $\alpha_{\Theta}^{\mathcal{F}}(\cdot)$  closely match the plots for  $\alpha_{\Gamma}^{\mathcal{F}}(\cdot)$  and  $\alpha_{\mathcal{A}}^{\mathcal{F}}(\cdot)$  for the four primary system  $\mathbf{P}_R^{(4)}$ . The corresponding renderings of the gray axis produced in the presence of primary variation are practically the same as the rendering on the display without primary variations. For the six primary system  $\mathbf{P}_U^{(6)}$ , Fig. S.3(b) shows that  $\alpha_{\Theta}^{\mathcal{F}}(\cdot)$  differs from  $\alpha_{\Gamma}^{\mathcal{F}}(\cdot)$  and  $\alpha_{\mathcal{A}}^{\mathcal{F}}(\cdot)$ , specially in the  $\beta_2$  component, and this difference is expressed (in the presence of primary variations) as the green hue shown in the stripe rendered by  $\alpha_{\Theta}^{\mathcal{F}}(\cdot)$ , causing deviations from neutrality for the rendered gray axis.

Figure S.4 shows the renderings for the trajectory defined by the radial line in CIELUV at constant lightness,  $\tau_L = 75$ , and opposing CIELUV hues corresponding to  $h_{\mathcal{T}} = 86^\circ$  and  $h_{\mathcal{T}} = 266^\circ$  for the six primary system  $\mathbf{P}_U^{(6)}$ . Since this trajectory corresponds to a line segment varying along chroma for two complementary hues, results in Fig. S.4 are shown as functions of chroma  $C_{\mathcal{T}}$ . To distinguish between the two hues, we add a negative sign to the chroma values for the points with  $h_{\mathcal{T}} = 266^\circ$ , leaving a positive sign for the points with  $h_{\mathcal{T}} = 86^\circ$ . In the plots for the CBS visualization and perceptual error, we also indicate with a gray shadowed box the color regions that fall outside the sRGB gamut. For visual assessment, the stripes representing the renderings are obtained by uniformly scaling the chroma of the renderings to fit inside the sRGB gamut. As this operation is performed in a perceptually uniform space, relative comparisons between scaled colors are still perceptually meaningful.

From Fig. S.4, the CBS components of the transition preserving CCFs  $\alpha_{\Theta}^{\mathcal{F}}(\cdot)$  and  $\alpha_{\Gamma}^{\mathcal{F}}(\cdot)$  match each other along the entire trajectory. A discontinuity in the first-order derivatives of  $\alpha_{\mathcal{A}}^{\mathcal{F}}(\cdot)$  appears at a color with high chroma  $C_{\mathcal{T}}$  and  $h_{\mathcal{T}} = 86^\circ$ . Around that point, color artifacts can be seen in the renditions produced by  $\alpha_{\mathcal{A}}^{\mathcal{F}}(\cdot)$  on the displays with primary variations. The artifacts are more prominent for  $\mathbf{P}_M^{(5)}$ , as a consequence of a strong change in the  $\beta_2$  component of  $\alpha_{\mathcal{A}}^{\mathcal{F}}(\cdot)$ , as shown in Fig. S.4.

Figure S.5 shows the renderings of the locus of constant chromaticity for (a)  $[x, y] = [0.3917, 0.4755]$  and (b)  $[x, y] = [0.3304, 0.3095]$  for the display system specified by  $\mathbf{P}_R^{(4)}$ . As expected from the theoretical results established in the Part I paper [8], the display renderings by  $\alpha_{\mathcal{A}}^{\mathcal{F}}(\cdot)$  for these color trajectories have constant chromaticity regardless of the primary variation. From Fig. S.5, note that for both loci the CCFs  $\alpha_{\Gamma}(\cdot)$  and  $\alpha_{\Theta}(\cdot)$  are practically the same, and that they differ from the loci for  $\alpha_{\mathcal{A}}(\cdot)$ . These differences increase for points in the

<sup>1</sup>The specific primary variations are tabulated in Table S.II.

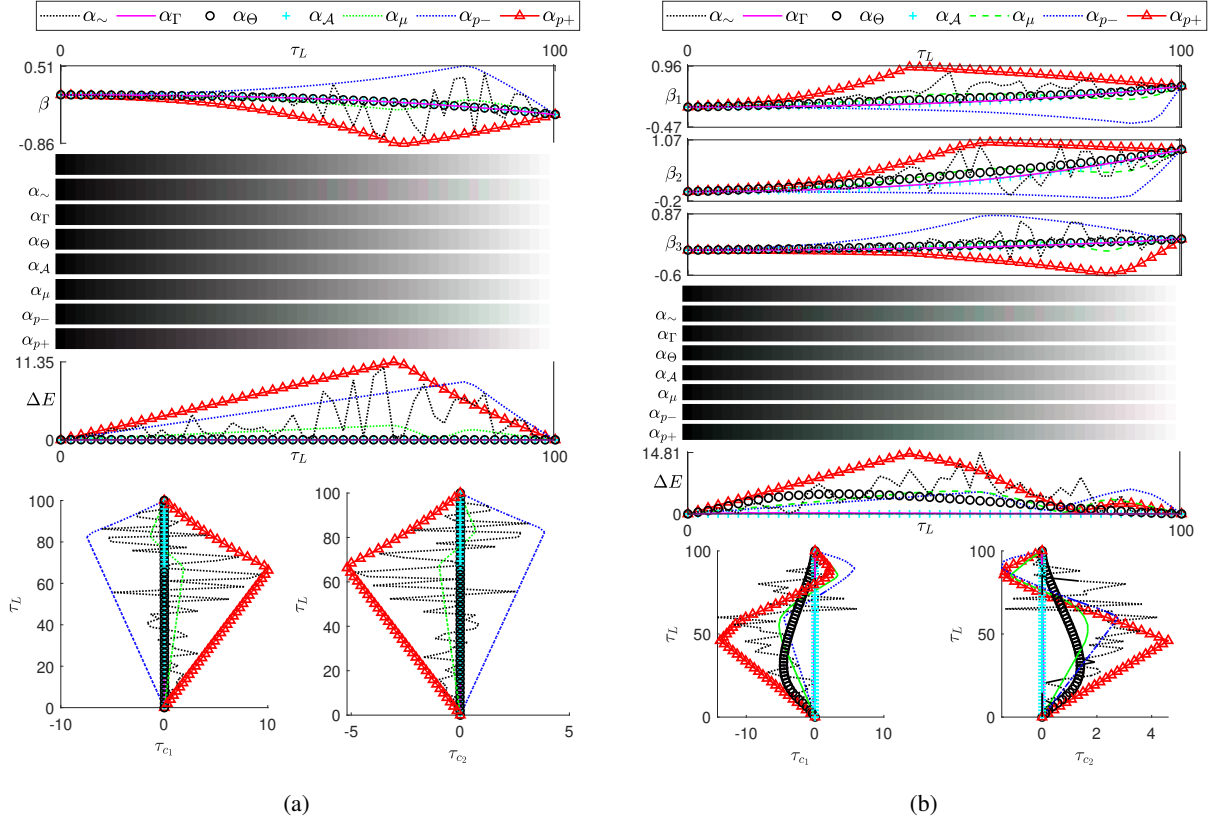


Fig. S.3: Rendered gray axis for (a) the four primary system  $\mathbf{P}_R^{(4)}$  and (b) the six primary system  $\mathbf{P}_U^{(6)}$ . The CCFs are evaluated on 50 uniformly spaced samples along the ramp. For each of the subfigures (a) and (b), the following are presented, in order, from top to bottom: (1) legend labels identifying the alternative CCFs considered, (2) visualization of the CCFs in the CBS as function of lightness  $\tau_L$ , (3) rendering of the gray ramp, (4) the perceptual color difference  $\Delta E(\cdot)$  between the system with the nominal primary and the one with the primary variation, and (5)  $\tau_L - \tau_{c_1}$ -plane and  $\tau_L - \tau_{c_2}$ -plane plots depicting the desired ramp (in black) and the renderings obtained with the alternative CCFs in the presence of the primary variation. **To appreciate the color differences, please see the electronic version of the document.**

interior of the gamut, while they are zero at the gamut surface (the extremes of the stripes). Note also that for these particular trajectories, color differences with respect to the rendering by the nominal display are higher for  $\alpha_{\mathcal{A}}^{\mathcal{F}}(\cdot)$  than the differences obtained with the transition preserving CCFs  $\alpha_{\Gamma}^{\mathcal{F}}(\cdot)$  and  $\alpha_{\Theta}^{\mathcal{F}}(\cdot)$ . Similar to the gray axis, the maximum error along the loci of constant chromaticity is also attained by one of the optimal power CCFs, while the random CCF exhibits numerous artifacts along the trajectory.

The trends in Figs. S.3–S.5 are in agreement with those presented in the main paper and further support the conclusions therein.

## S. VI. RESULTS FOR ADDITIONAL PRIMARY SYSTEMS

The results presented in the main paper [1] and in Section S.V consider display systems where each primary expands the chromaticity gamut beyond what the other primaries would provide. Alternative designs that do not exhibit this chromaticity expansion behavior have, however, also been used in practice. For example, four primary

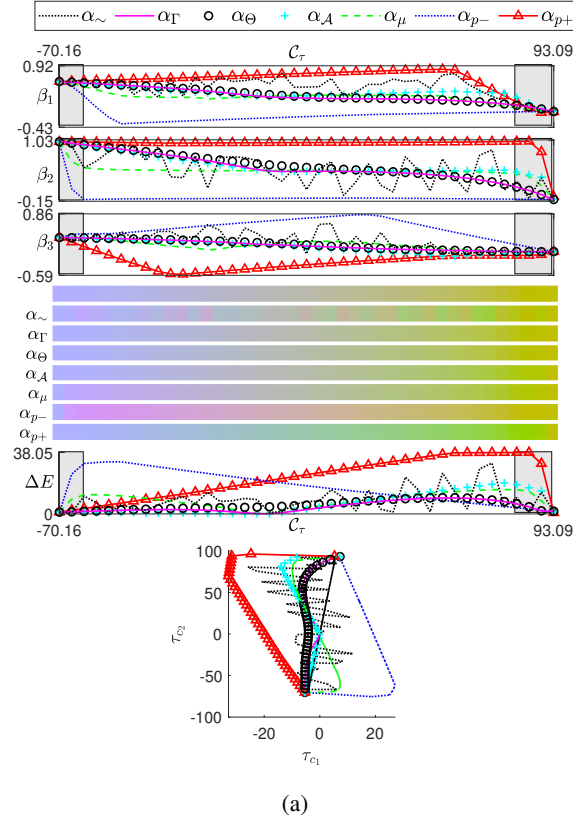


Fig. S.4: Radial line in CIELUV at constant lightness,  $\tau_L = 75$ , and opposing CIELUV hues corresponding to  $h_{\mathcal{T}} = 86^\circ$  and  $h_{\mathcal{T}} = 266^\circ$ , for the six primary system  $\mathbf{P}_U^{(6)}$ . The CCFs are evaluated on 40 uniformly spaced samples between the two extreme points on the gamut surface. From top to bottom: (1) legend labels identifying the alternative CCFs considered, (2) visualization of the CCFs in the CBS as function of chroma  $C_{\mathcal{T}}$ , (3) rendering of the ramp between the maximum chroma values for the two opposing hues  $h_{\mathcal{T}} = 86^\circ/266^\circ$ , (4) the perceptual color difference  $\Delta E(\cdot)$  between the system with the nominal primary and the one with the primary variation, and (5)  $\tau_{c_1} - \tau_{c_2}$ -plane plot depicting the desired ramp (in black) and the renderings obtained with the alternative CCFs in the presence of the primary variation. For the purpose of illustration, chroma values along the two opposing hues  $h_{\mathcal{T}} = 86^\circ/266^\circ$  are assigned positive and negative signs, respectively. The transparent gray boxes overlaid on the two ends identify the regions outside the sRGB gamut. **To appreciate the color differences, please see the electronic version of the document.**

display systems where the added primary is white (and therefore does not expand the chromaticity gamut) have been used in some designs for increasing the display white luminance. The analysis in the Part I paper [8] and the methodology proposed in the Part II paper [1] are general and also apply to these and other alternative designs. To illustrate this broader applicability of the proposed framework, in this section, we present additional results for two additional primary systems: a four primary system  $\mathbf{P}_C^{(4)}$ , where the added primary is a white primary and a six primary system  $\mathbf{P}_S^{(6)}$ , with one pair each of red, green, blue primaries, where the primaries within a pair include one saturated primary and one desaturated primary, both having the same dominant wavelength [9, pp. 175-176]. The primaries for these systems are specified in Table S.VII and we outline how these were chosen in the next two paragraphs.

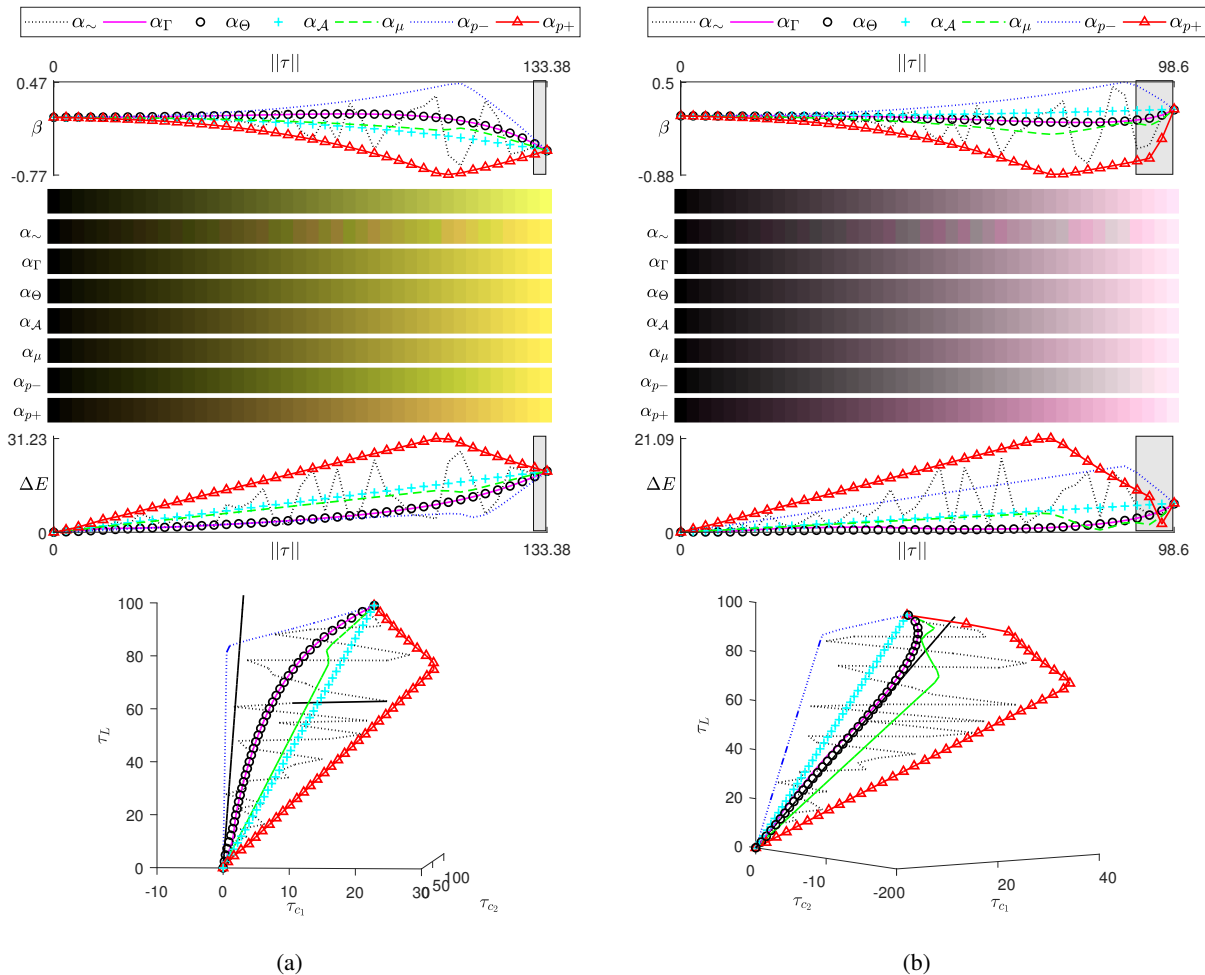


Fig. S.5: Loci of constant chromaticity, (a)  $x = 0.3917, y = 0.4755$  and (b)  $x = 0.3304, y = 0.3095$ , for the four primary system  $\mathbf{P}_R^{(4)}$ . The CCFs are evaluated on 40 uniformly spaced samples between the two extreme points on the gamut surface. For each of the subfigures (a) and (b), the following are presented, in order, from top to bottom: (1) legend labels identifying the alternative CCFs considered, (2) visualization of the CCFs in the CBS as function of the norm  $\|\tau\|$ , (3) rendering of the loci, (4) the perceptual color difference  $\Delta E(\cdot)$  between the system with the nominal primary and the one with the primary variation, and (5)  $\tau_L, \tau_{c_1}, \tau_{c_2}$  plot depicting the desired ramp (in black) and the renderings obtained with the alternative CCFs in the presence of the primary variation. The transparent gray boxes overlaid on the two ends identify the regions outside the sRGB gamut. **To appreciate the color differences, please see the electronic version of the document**

The chromaticity gamut and the power spectral distribution of the four primaries of  $\mathbf{P}_C^{(4)}$  are shown in Fig.S.6. Note that the chromaticity for the first three primaries of  $\mathbf{P}_C^{(4)}$  match the sRGB specifications [10], while the fourth primary matches the chromaticity of white at a luminance set to 30% of the luminance of the composite RGB white formed by the sRGB primaries. Similarly, Fig. S.6 shows the chromaticity gamut and the power spectral distribution of the primaries of  $\mathbf{P}_S^{(6)}$ . The six primaries comprise one pair each of red, green, blue primaries, where the primaries within a pair are matched in dominant wavelength [9, pp. 175-176]<sup>2</sup> with one having a narrow-band spectrum and

<sup>2</sup>Primaries with a matching dominant wavelength have chromaticities located along a radial line emanating from the white point in the CIE  $xy$  plane.

the other having a wider band spectrum. The first three primaries match the REC2020 specifications [11], which can be realized as narrow-band spectra emitted by lasers. The chromaticity for the remaining three primaries match the dominant wavelength of corresponding REC2020 primaries and can be realized as wider spectral distributions emitted by LEDs. Results characterizing the robustness of alternative CCFs to primary variations<sup>3</sup> for both systems are shown in Tables S.VIII and S.IX and exhibit the same trends as the other systems previously analyzed.

Figure S.8 shows the renderings of the four primary system  $\mathbf{P}_C^{(4)}$  for the two radial lines in CIELUV at constant lightness,  $\tau_L = 75$ , and opposing CIELUV hues corresponding to  $h_{\tau} = 45^\circ$  and  $h_{\tau} = 225^\circ$ , and the opposing hues  $h_{\tau} = 45^\circ$  and  $h_{\tau} = 225^\circ$ , shown in Fig. S.8(a) and Fig. S.8(b), respectively. Similarly, Fig. S.9 shows the renderings of the six primary system  $\mathbf{P}_S^{(6)}$  for the two radial lines in CIELUV at constant lightness,  $\tau_L = 75$ , and opposing CIELUV hues corresponding to  $h_{\tau} = 63^\circ$  and  $h_{\tau} = 243^\circ$ , and the opposing hues  $h_{\tau} = 153^\circ$  and  $h_{\tau} = 333^\circ$ , shown in Fig. S.8(a) and Fig. S.8(b), respectively. These renderings correspond to primary variations for  $\mathbf{P}_C^{(4)}$  and  $\mathbf{P}_S^{(6)}$  as listed in Table S.X, where the corresponding figures with the visual examples are also identified. For visualization of the CCFs, we used the vectors shown in Table S.XI as basis of the CBS for the primary systems.

In agreement with results shown in main paper and in the supplementary materials, Figs. S.8 and S.9 show that the CBS components of the transition preserving CCFs  $\alpha_{\Theta}^{\mathcal{F}}(\cdot)$  and  $\alpha_{\Gamma}^{\mathcal{F}}(\cdot)$  match each other along all the trajectories. Points of derivative discontinuity in the axially linear CCF  $\alpha_{\mathcal{A}}^{\mathcal{F}}(\cdot)$  can be seen in the plots of the CBS components and in each case, corresponding artifacts can be seen in the renderings. Specifically, the derivative discontinuity is manifested in the rendering as a localized change in the perceived gradients which is subtle in Fig. S.8 and quite prominent in Fig. S.9, aligned with the broader trend already noted that the artifacts become more prominent with increasing number of primaries  $K$ . The optimal power CCFs  $\alpha_{p-}^{\mathcal{F}}(\cdot)$  and  $\alpha_{p-}^{\mathcal{F}}(\cdot)$  show much higher sensitivity to primary variations than the proposed optimal CCFs  $\alpha_{\Theta}^{\mathcal{F}}(\cdot)$  and  $\alpha_{\Gamma}^{\mathcal{F}}(\cdot)$  and the axially linear CCF  $\alpha_{\mathcal{A}}^{\mathcal{F}}(\cdot)$ .

Both the numerical results and the visual examples for these additional systems align with the results presented in the main paper and highlight the general applicability and utility of the proposed framework.

		$\mathbf{P}_1$	$\mathbf{P}_2$	$\mathbf{P}_3$	$\mathbf{P}_4$	$\mathbf{P}_5$	$\mathbf{P}_6$
$\mathbf{P}_C^{(4)}$	X	0.4124	0.3576	0.1805	0.2851		
	Y	0.2126	0.7152	0.0722	0.3000		
	Z	0.0193	0.1192	0.9505	0.3267		
		$\mathbf{P}_1$	$\mathbf{P}_2$	$\mathbf{P}_3$	$\mathbf{P}_4$	$\mathbf{P}_5$	$\mathbf{P}_6$
$\mathbf{P}_U^{(6)}$	X	50.9566	11.5694	13.5105	10.4096	3.4197	5.1798
	Y	21.0160	54.2398	4.7441	5.5336	10.5909	3.8755
	Z	0.0000	2.2458	84.8788	2.2217	2.0881	17.4713

TABLE S.VII: Tristimulus values of the primaries of the display systems  $\mathbf{P}_C^{(4)}$  and  $\mathbf{P}_S^{(6)}$ .

<sup>3</sup>The Monte Carlo methodology outlined in the main paper was also used for these primary sets.

		$\mathbf{P}_C^{(4)}$									
		$\Theta^*$	$\mathcal{M}_\Theta^*$	$\Delta E_{uv}^*$		$\Delta E_{ab}^*$		$\Delta E_{00}^*$		$\Delta E_{16}$	
CCF			max	av.	max	av.	max	av.	max	av.	max
$\alpha_{\sim}^{\mathcal{F}}$		0.6047	8.6308	2.09	23.15	1.83	19.91	2.28	17.59	1.88	7.35
$\alpha_{\Gamma}^{\mathcal{F}}$		0.0013	0.7432	0.03	0.12	0.03	0.19	0.04	0.27	0.16	1.08
$\alpha_{\Theta}^{\mathcal{F}}$		0.0000	0.0000	0.30	1.72	0.25	1.52	0.35	2.12	0.60	2.45
$\alpha_{\mathcal{A}}^{\mathcal{F}}$		0.0497	1.6163	0.00	0.00	0.00	0.00	0.00	0.00	0.00	0.00
$\alpha_{\mu}^{\mathcal{F}}$		0.0783	1.6378	1.31	9.94	1.12	8.18	1.49	9.46	1.48	4.60
$\alpha_{p-}^{\mathcal{F}}$		0.1892	1.6163	4.03	27.91	3.45	23.39	4.09	19.24	2.79	7.78
$\alpha_{p+}^{\mathcal{F}}$		0.3363	2.0581	2.11	14.45	1.68	10.63	2.17	11.52	1.89	5.58
$\Theta_{\mathcal{V}_{\mathcal{F}}}(\alpha_{\Theta}^{\mathcal{F}})$							0.0305				
$\mathcal{V}_{\mathcal{F}}$							1200005				

TABLE S.VIII: Quantitative metrics for alternative CCFs for the  $K = 4$  primary display system  $\mathbf{P}_C^{(4)}$ .

		$\mathbf{P}_S^{(6)}$									
		$\Theta^*$	$\mathcal{M}_\Theta^*$	$\Delta E_{uv}^*$		$\Delta E_{ab}^*$		$\Delta E_{00}^*$		$\Delta E_{16}$	
CCF			max	av.	max	av.	max	av.	max	av.	max
$\alpha_{\sim}^{\mathcal{F}}$		0.5462	8.2855	1.78	18.08	1.53	15.15	1.97	14.82	1.78	6.75
$\alpha_{\Gamma}^{\mathcal{F}}$		0.0001	0.4275	0.02	0.19	0.02	0.13	0.03	0.20	0.12	0.44
$\alpha_{\Theta}^{\mathcal{F}}$		0.0000	0.0000	0.04	0.34	0.03	0.24	0.05	0.36	0.17	0.65
$\alpha_{\mathcal{A}}^{\mathcal{F}}$		0.1489	8.9514	0.00	0.00	0.00	0.00	0.00	0.00	0.00	0.00
$\alpha_{\mu}^{\mathcal{F}}$		0.2130	6.6298	1.23	8.91	1.07	7.32	1.43	8.74	1.45	4.78
$\alpha_{p-}^{\mathcal{F}}$		0.6534	14.3024	2.11	10.78	1.76	9.04	2.29	10.23	1.98	5.40
$\alpha_{p+}^{\mathcal{F}}$		0.6719	16.5152	2.96	20.22	2.54	17.01	3.14	16.05	2.39	7.17
$\Theta_{\mathcal{V}_{\mathcal{F}}}(\alpha_{\Theta}^{\mathcal{F}})$							0.0513				
$\mathcal{V}_{\mathcal{F}}$							2480649				

TABLE S.IX: Quantitative metrics for alternative CCFs for the  $K = 6$  primary display system  $\mathbf{P}_S^{(6)}$ .

		$\Delta \mathbf{p}_1$	$\Delta \mathbf{p}_2$	$\Delta \mathbf{p}_3$	$\Delta \mathbf{p}_4$	$\Delta \mathbf{p}_5$	$\Delta \mathbf{p}_6$
$\Delta \mathbf{P}_C^{(4)}$ Fig S.8(a)	X	0.0260	0.0467	0.0599	-0.0395		
	Y	-0.0383	-0.0657	-0.0762	0.0348		
	Z	-0.0011	-0.0032	-0.0009	-0.0002		
$\Delta \mathbf{P}_C^{(4)}$ Fig S.8(b)	X	0.0302	0.0455	0.0581	-0.0395		
	Y	-0.0351	-0.0667	-0.0776	0.0348		
	Z	0.0024	0.0004	-0.0003	-0.0009		
$\Delta \mathbf{P}_S^{(6)}$ Fig S.9	X	9.0435	4.2502	-5.0570	-1.7291	-2.7226	3.8999
	Y	-9.1573	-7.9337	2.9464	1.1716	2.5630	0.6093
	Z	-1.1009	4.8507	0.2041	1.6015	0.4324	-0.8318

TABLE S.X: Variations in the primaries  $\mathbf{P}_C^{(4)}$  and  $\mathbf{P}_S^{(6)}$  used for the assessments of CCF robustness in the visual examples. The table also identifies the figures where visual examples were presented using the corresponding primary variations.

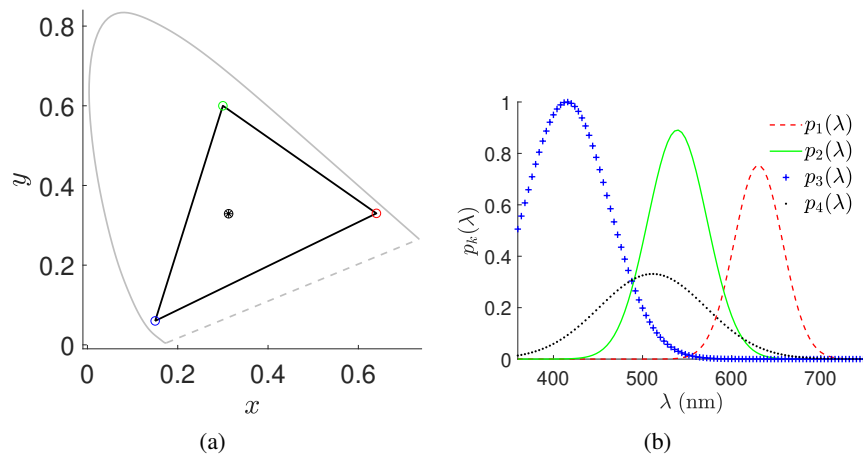


Fig. S.6: For the four-primary system  $\mathbf{P}_C^{(4)}$  the figure shows: (a) The chromaticity of the primaries (circles) and display white (black asterisk), and the chromaticity gamut (black solid triangle). The chromaticity for the first three primaries match the sRGB specifications [10], while the chromaticity of the fourth primary matches the white point. (b) The normalized spectral power distribution for the primaries modeled as Gaussian functions that approximate the spectra of LEDs.

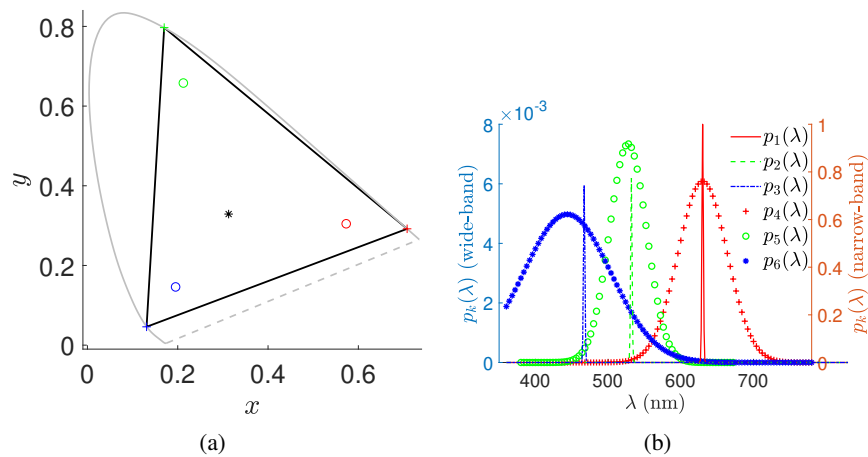


Fig. S.7: For the six-primary system  $\mathbf{P}_S^{(6)}$  the figure shows: (a) The chromaticity of the primaries (scattered circles and pluses) and display white (black asterisk), and the chromaticity gamut (black solid line). The chromaticity of the first set of three primaries match the REC2020 specifications [11] (pluses), while the chromaticity for the second set of primaries is a less saturated, matching of the dominant wavelength of the REC2020 primaries (circles). (b) The spectral power distribution for the primaries. The first three primaries with narrow-band emission spectra can be realized using lasers, while the remaining three primaries with wider spectral emission distributions can be realized using LEDs.

	$\mathbf{b}_1$	$\mathbf{b}_2$	$\mathbf{b}_3$
$\mathbf{B}_C^{(4)}$	-0.2662		
	-0.2662		
	-0.2662		
	0.8874		
$\mathbf{B}_S^{(6)}$	-0.9522	-0.1258	-0.1273
	0.1329	-0.9600	0.0601
	0.1512	-0.0201	-0.9515
	0.2292	0.0576	0.0789
	-0.0082	0.2401	0.0379
	-0.0122	0.0345	0.2592

TABLE S.XI: Orthonormal basis for the CBS of the multiprimary displays  $\mathbf{P}_C^{(4)}$  and  $\mathbf{P}_S^{(6)}$  used in the visualization of the CCFs.

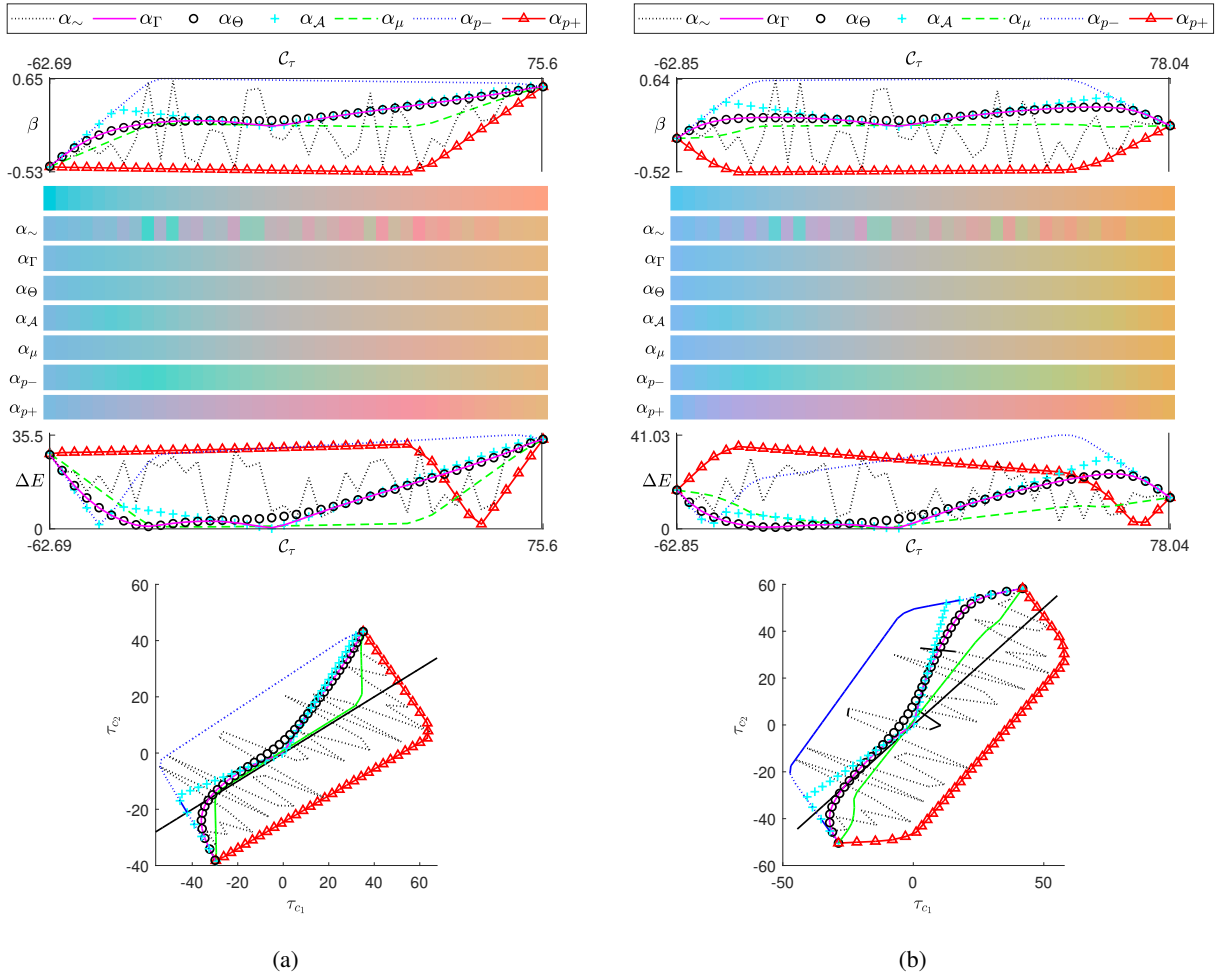


Fig. S.8: Radial line in CIELUV at constant lightness,  $\tau_L = 75$ , and (a) opposing CIELUV hues corresponding to  $h_{\mathcal{T}} = 63^\circ$  and  $h_{\mathcal{T}} = 243^\circ$ , (b) opposing CIELUV hues corresponding to  $h_{\mathcal{T}} = 45^\circ$  and  $h_{\mathcal{T}} = 225^\circ$ , for the four primary system  $\mathbf{P}_C^{(4)}$ . The CCFs are evaluated on 40 uniformly spaced samples between the two extreme points on the gamut surface. From top to bottom: (1) legend labels identifying the alternative CCFs considered, (2) visualization of the CCFs in the CBS as function of chroma  $C_{\mathcal{T}}$ , (3) rendering of the ramp between the maximum chroma values for the two opposing hues, (4) the perceptual color difference  $\Delta E(\cdot)$  between the system with the nominal primary and the one with the primary variation, and (5)  $\tau_{c_1} - \tau_{c_2}$ -plane plot depicting the desired ramp (in black) and the renderings obtained with the alternative CCFs in the presence of the primary variation. For the purpose of illustration, chroma values along the two opposing hues, for (a)  $h_{\mathcal{T}} = 63^\circ/h_{\mathcal{T}} = 243^\circ$  and for (b)  $h_{\mathcal{T}} = 45^\circ/h_{\mathcal{T}} = 225^\circ$ , are assigned positive and negative signs, respectively. **To appreciate the color differences, please see the electronic version of the document.**

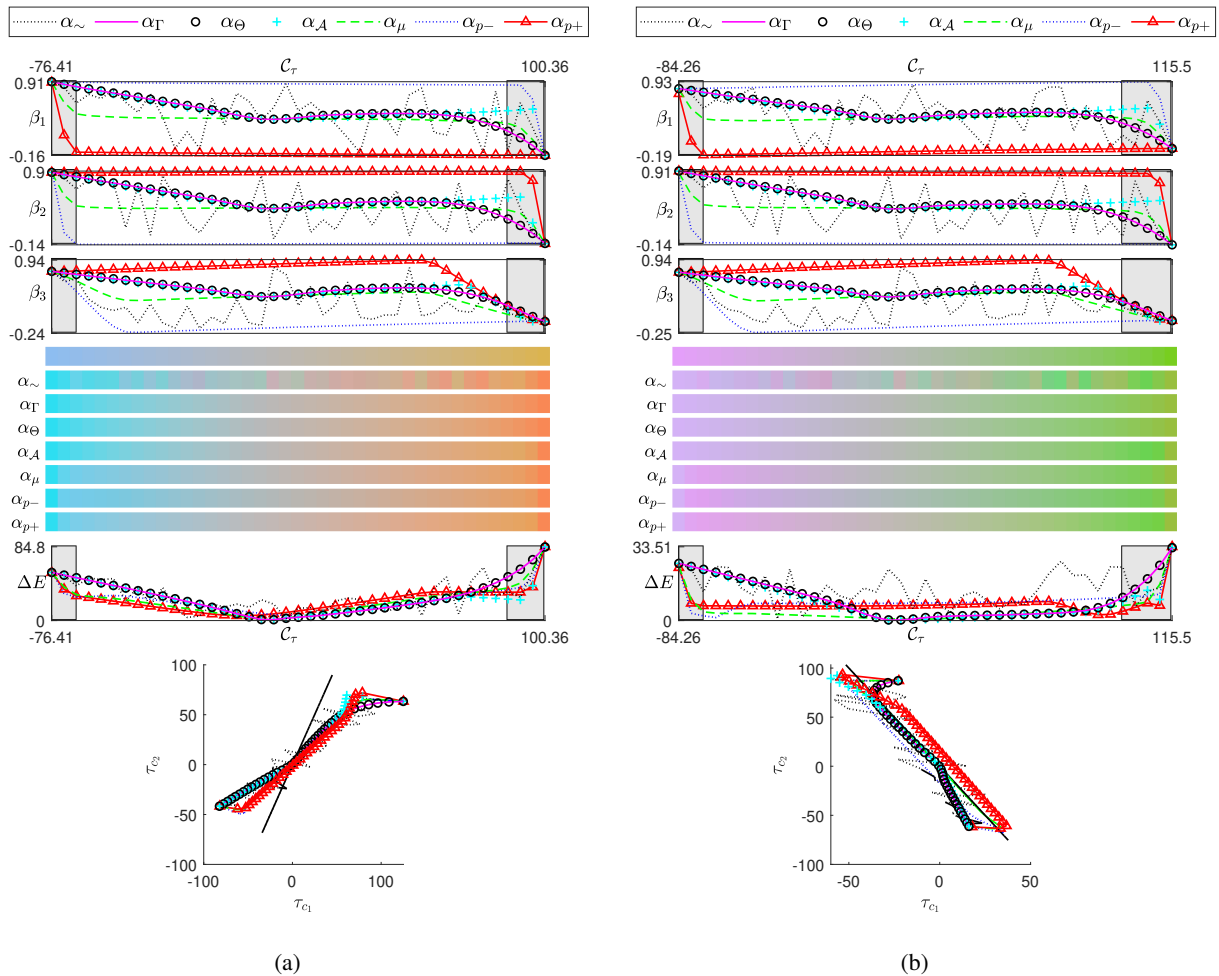


Fig. S.9: Radial line in CIELUV at constant lightness,  $\tau_L = 75$ , and (a) opposing CIELUV hues corresponding to  $h_{\mathcal{T}} = 63^\circ$  and  $h_{\mathcal{T}} = 243^\circ$ , (b) opposing CIELUV hues corresponding to  $h_{\mathcal{T}} = 153^\circ$  and  $h_{\mathcal{T}} = 333^\circ$ , for the six primary system  $\mathbf{P}_S^{(6)}$ . The CCFs are evaluated on 40 uniformly spaced samples between the two extreme points on the gamut surface. From top to bottom: (1) legend labels identifying the alternative CCFs considered, (2) visualization of the CCFs in the CBS as function of chroma  $C_{\mathcal{T}}$ , (3) rendering of the ramp between the maximum chroma values for the two opposing hues, (4) the perceptual color difference  $\Delta E(\cdot)$  between the system with the nominal primary and the one with the primary variation, and (5)  $\tau_{c_1} - \tau_{c_2}$ -plane plot depicting the desired ramp (in black) and the renderings obtained with the alternative CCFs in the presence of the primary variation. For the purpose of illustration, chroma values along the two opposing hues, for (a)  $h_{\mathcal{T}} = 63^\circ/h_{\mathcal{T}} = 243^\circ$  and for (b)  $h_{\mathcal{T}} = 153^\circ/h_{\mathcal{T}} = 333^\circ$ , are assigned positive and negative signs, respectively. The transparent gray boxes overlaid on the two ends identify the regions outside the sRGB gamut. **To appreciate the color differences, please see the electronic version of the document.**

## REFERENCES

- [1] C. E. Rodríguez-Pardo and G. Sharma, "Color control functions for multiprimary displays II: Variational robustness optimization," *IEEE Trans. Image Proc.*, vol. 28, 2019. [Online]. Available: <https://doi.org/10.1109/TIP.2019.2936992>
- [2] G. H. Golub and C. F. V. Loan, *Matrix Computations*, 2nd ed. Baltimore, MD: The Johns Hopkins University Press, 1989.
- [3] CIE, "Colorimetry," CIE Publication No. 15.2, Central Bureau of the CIE, Vienna, 1986, the commonly used data on color matching functions is available at the CIE web site at <http://www.cie.co.at/>.
- [4] CIE, "Improvement to industrial colour-difference evaluation," CIE Publication No. 142-2001, Central Bureau of the CIE, Vienna, 2001.
- [5] M. R. Luo, G. Cui, and B. Rigg, "The development of the CIE 2000 colour-difference formula: CIEDE2000," *Color Res. Appl.*, vol. 26, no. 5, pp. 340–350, Oct. 2001.
- [6] G. Sharma, W. Wu, and E. N. Dalal, "The CIEDE2000 color-difference formula: Implementation notes, supplementary test data, and mathematical observations," *Color Res. Appl.*, vol. 30, no. 1, pp. 21–30, Feb. 2005.
- [7] C. Li, Z. Li, Z. Wang, Y. Xu, M. R. Luo, G. Cui, M. Melgosa, M. H. Brill, and M. Pointer, "Comprehensive color solutions: CAM16, CAT16, and CAM16-UCS," *Color Res. Appl.*, vol. 42, no. 6, pp. 703–718, 2017.
- [8] C. E. Rodríguez-Pardo and G. Sharma, "Color Control Functions for Multiprimary Displays I: Robustness Analysis and Optimization Formulations," *IEEE Trans. Image Proc.*, vol. 28, 2019. [Online]. Available: <https://doi.org/10.1109/TIP.2019.2937067>
- [9] G. Wyszecki and W. S. Stiles, *Color Science: Concepts and Methods, Quantitative Data and Formulae*, 2nd ed. New York: John Wiley & Sons, Inc., 1982.
- [10] IEC, "Colour measurement and management in multimedia systems and equipment, part 2-1: Colour management - default RGB colour space- sRGB," IEC Publication No. 61966-2.1, 1999.
- [11] I. T. Union, "Recommendation ITU-R BT. 2020-2. parameter values for UHD TV systems for production and international programme exchange," <https://www.itu.int/rec/R-REC-BT.2020/>, Oct. 2015.